Senior Thesis

Three's A Cloud: an Analysis of Spectral Variability in SIMPJ013656.57+093347.3 Over Three Epochs of Hubble Space Telescope Observations

by Jumi Hall

May 14, 2024

Project Instructor: Dr. Yifan Zhou
Department of Astronomy
University of Virginia
This thesis is submitted in partial completion of the requirements of the BA Astronomy Major.

Abstract

This thesis analyzes time-resolved spectra acquired over three time periods of data gathered from brown dwarf SIMPJ013656.57+093347.3 (SIMPJ0136 for short). It begins with an overview of exoplanet discovery methods and the value of brown dwarf atmospheric analysis on exoplanetary science. Specifically, we find that the atmosphere of SIMPJ0136 most resembles those of directly imaged planets. This leads to a summary of past findings concerning the brown dwarf SIMPJ0136, which includes conclusions from the paper whose data we re-analyze and replicate along with 2 other epochs' data. Then, spectral information is integrated over a range of wavelengths, producing light curves. Rotational modulations found in the light curves support a 2.4-hour period of rotation and the possibility of cloud structures. Phase-folded light curves from the three epochs are created, along with plots of the maximum and minimum spectra from each epoch. With data from the three epochs, we create a simple 2D plot of light flux produced from a blackbody to explore how a cold spot's temperature and coverage percentage may change the flux produced. Models of brown dwarf atmospheres with different temperatures and thicknesses are compared against our observational data, and the chi-square formula is used to determine the model of best fit. The model is then improved upon to find exact variations of cloud thickness and temperature in the atmosphere. Through light curve analysis, spectral ratio analyses, and best-fit modeling, this thesis concludes that the long-term variability present between the epochs does not exceed the rotational modulation of the epochs themselves. It concludes that over three epochs, the majority of the atmosphere on SIMPJ0136 consists of thin clouds at a temperature of 1200 Kelvin, with a patch of thick clouds covering 12 percent of one hemisphere in Epochs 1 and 2, and 6 percent of one hemisphere in Epoch 3.

Contents

List of Figures

1 Introduction

1.1 Exoplanet Discovery

Exoplanet discovery and analysis is a rapidly expanding field in astronomy, with new planets being discovered at an unprecedented rate. This can be qualitatively seen by the difference in Figures 1 and 2, which highlight the increase in confirmed planets between 2017 and 2023. Figure 1, featured in the Exoplanet Handbook in 2017, shows exoplanets from NASA's 2017 exoplanet archive whose masses were plotted against their determined orbital periods [1].

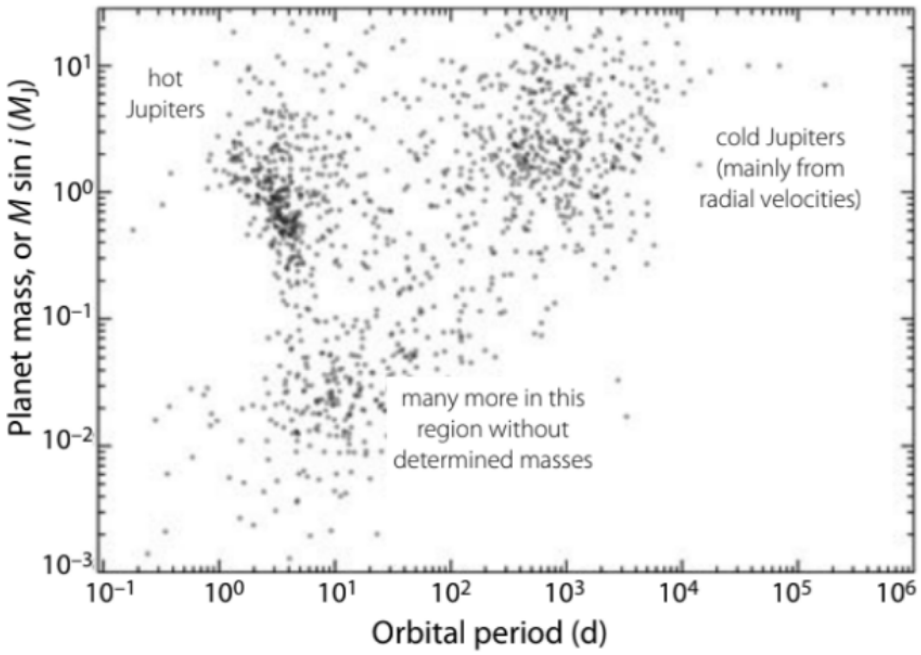

Figure 1: Planet Mass vs. Orbital Periods from the 2017 Exoplanet Handbook [1]. Data was gathered from NASA's exoplanet archive in 2017. Only planets with both confirmed masses and orbital periods are included in the graph. Observational biases inflate the appearance of a relative abundance of large planets with short orbital periods. These planets are often found through the transiting method, while large planets far from their stars are found with the radial velocity method.

The recreation of this graph using updated data from NASA's 2023 exoplanet archive, shown in Figure 2 shows the massive increase in confirmed exoplanets over the last 6 years. The most rapidly growing discovery method, the transiting method, for example, saw an increase of over 1,890 new exoplanets.

The detection methods are also added to this graph, showing the types of planets most likely to be observed through different methods of observation. As shown in the graph, exoplanet discovery is dominated by radial velocity and transit detection methods, which are best at finding planets with large masses, or planets with rapid periods of revolution, both not helpful in discovering Earth-like or habitable planets. Although brown dwarfs cannot be placed on this graph due to their lack of an observable orbital period (given that they do not revolve around a star), their atmospheres are useful to analyze because of their easily obtained spectra and resemblance to massive and hot planets.

To visualize the relation of brown dwarfs and observed exoplanet data, we create another graph, shown in Figure 3. Again using the 2023 archive data, we plot planets' equilibrium temperatures against their planetary masses. Although this thesis focuses on the brown dwarf's effective temperature and not its equilibrium temperature, the equilibrium temperature dataset can be used, as the differences between the types of temperatures are minimal compared to the observational error in our dataset. Placing the brown dwarf at an equilibrium temperature of about 1200K and 13 Jupiter masses, we can determine that brown dwarfs are close analogs to directly imaged exoplanets [2].

This is valuable because, as indicated by Figures 2 and 3, discovering exoplanets through imaging is a less common method of detection due to its stringent requirements [3]. Brown dwarf spectra are more easily acquired and often have higher quality than those of planets detected with imaging due to their higher light emissions and the lack of a solar presence in their surroundings. This ease of data collection is why brown dwarf atmospheres are often studied as example atmospheres of exoplanets, such as in the work of Faherty et al. [4].

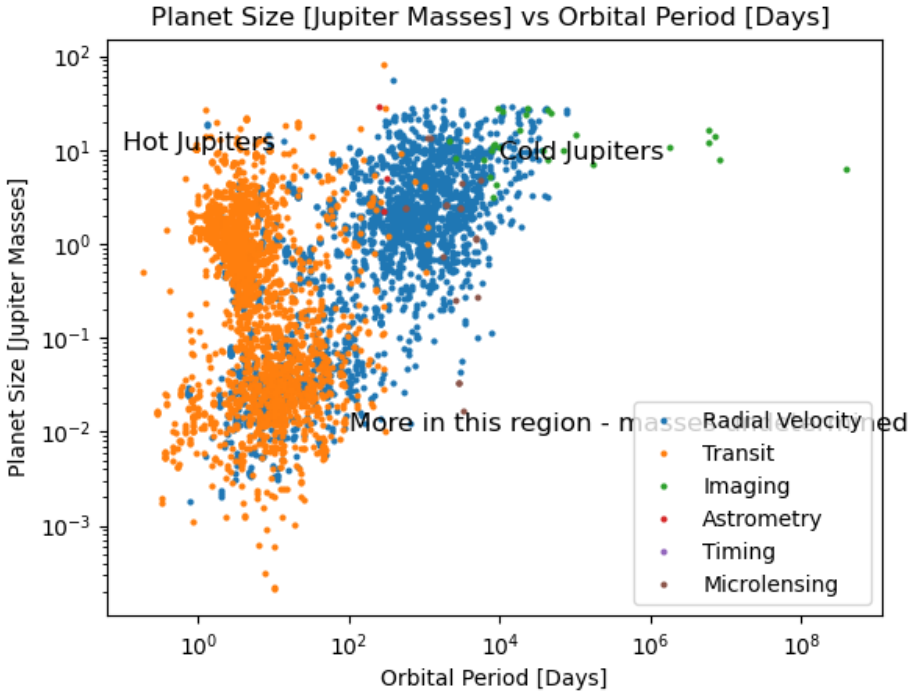

Figure 2: Graph of Planet Mass vs. Orbital Periods using NASA's exoplanet archive data from 2023. This recreation of the graph found in the 2017 Exoplanet Handbook emphasizes the rapid increase in exoplanet detections in the past 6 years. The planets are plotted by detection method, with detections from radial velocity and transit methods, in blue and orange respectively, making up most of the detections.

1.2 Atmospheres on Exoplanets

Through the various ways of exoplanet detection, astronomers have been able to not only gather data about their sizes and masses, but also their atmospheric compositions [6]. Atmospheric compositions are vital to the exploration of extrasolar planetary systems and our understanding of their

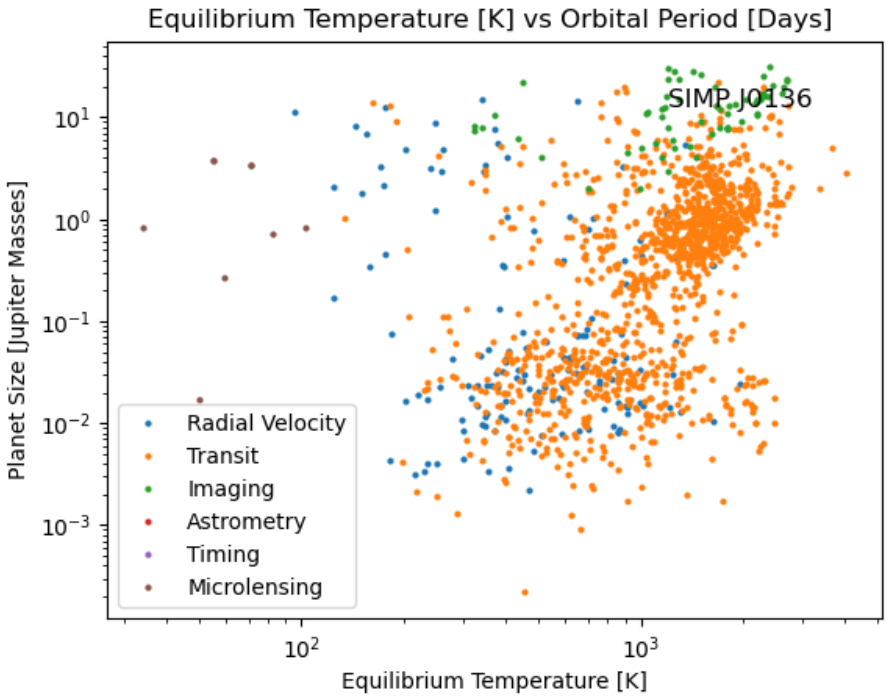

Figure 3: Graph of Planet Size vs. Equilibrium Temperatures using NASA's exoplanet archive data from 2023. SIMPJ0136 is plotted at a temperature of 1200K and 13 Jupiter masses, characteristics taken from the work of Gagne et al. [5]. The location aligns well with exoplanets detected through imaging methods. Thus, studying the atmosphere of this brown dwarf can lend insight into atmospheres of exoplanets usually detected through imaging.

evolutionary processes. Not only do they give data about planetary atmospheric compositions at different points in the lifespans of planets present in protoplanetary disks and around different types of stars, but the atmosphere is where scientists are looking for key biomarkers that would indicate extraterrestrial life.

Clouds and hazes in exoplanetary atmospheres can have wide ranges of temperatures, contents, and conditions [7]. Cloud models indicate a variety of effects from these wide-ranging atmospheric possibilities [7]. For example, they can decrease or increase the equilibrium temperature of a planet, or heat or cool the atmosphere in a greenhouse effect or "anti-greenhouse effect" [7]. With transiting planets, the atmosphere will affect the transmission spectra to follow a variation of planet radius with wavelength observed, as the atmosphere will be opaque at some wavelengths. With directly imaged planets, young Jupiters can be observed to have clouds if their temperatures vary from what is expected from a cloudless atmosphere. The latter methodology is what will be used in this thesis to determine the atmospheric composition of our observed brown dwarf.

1.3 SIMP J0136

The brown dwarf that we will be studying is named SIMP J013656.57+093347.3, which will be referred to simply as SIMPJ0136 in this paper. SIMPJ0136 has been studied over the course of many years, starting in 2009 with a team of researchers obtaining hours of continuous photometry

from the brown dwarf over the course of 4 nights [8]. This team determined some key characteristics about the brown dwarf, which include its relatively fast 2.4hr period of rotation, and its light curve variations that pointed to the presence of what they termed "J-term brightening". J term brightening refers to the unexpected inverse correlation between J-band luminosity and temperature of brown dwarfs straddling the L/T transition. In the transitional region between the hotter L-type brown dwarf and the cooler T-type brown dwarf, it would be expected that the brown dwarf would emit less infrared light than actually measured in observations [8]. Instead, near-infrared brightness increases as the temperature decreases. This indicates a possibility of cloudy atmospheres, which would decrease observed brightness.

Artigau et al. detected significant photometric variability in the infrared, implying a possible cloudy atmosphere. They derived three possible scenarios: dusty clouds on a clear atmosphere at the same temperature, inhomogeneous surface temperature, or dusty clouds on a clear atmosphere at different temperatures. Using models of different possible scenarios and the process of elimination, this group found a probable explanation for the intriguing characteristic to be an atmosphere consisting of regions with no grains, and regions with colder, grain-bearing clouds.

Then, in 2013, Apai et al. studied the same object, this time with the G141 spectrograph provided by the Hubble Space Telescope (HST). With the HST, these researchers implemented time-resolved near-infrared spectroscopy to produce light curves of the J and H bands, revealing similar conclusions about patchy cloud coverage on SIMPJ0136. Notably, this project used possible cloud coverage to explain the underluminosity problem posed by giant exoplanets, where most appear to be much fainter than expected when compared to brown dwarfs of the same spectral type [9]. After reducing the data and computing uncertainties from white noise and time-dependent trends, the period was calculated to be 2.39 hours, and spectral analysis began. Light curve analysis was performed through the spectral mapping routine Stratos, with which the light curves were reproduced with layers of thin, warm clouds, and cold, thick clouds. The formation of these thick clouds are theorized to be either circulation or large-scale vertical mixing. Importantly, this group found that there would be no regions without clouds on the brown dwarf [9]. This research paper will be the focus of the first section of this thesis, in which we will reanalyze their data, along with newer data from 2 other time periods.

In 2017, it was determined with a 99.9 percent probability that SIMPJ0136 was a member of the Carina-Near moving group, a group consisting of 8 core members and 10 probable members more loosely distributed [5]. The 200 +/- 50 Myr group was surveyed in the BANYAN All-Sky Survey-Ultracool, or BASS-Ultracool, and with cross-matching efforts from AllWISE and 2MASS sources, more precise parallax and motion measurements were able to be calculated, along with the determination that there is a low probability that SIMPJ0136 is a chance field interloper. Because SIMPJ0136 was found in this very young group, its mass could be calculated with more accuracy, leading to a result of around 12.7 M_{Jup}. Its radius was calculated to be 1.22 R_{Jup}, and its effective temperature 1096K. This information heightens the importance of this particular brown dwarf as an effective benchmark for giant gaseous exoplanetary atmospheres.

In 2018, Kao et al. studied SIMPJ0136 in radio wavelengths using the Very Large Array, which led to findings about its magnetic field pulses, revealing information about the importance of objects' rapid rotations in strong dipole fields [10]. The study of SIMPJ0136's magnetic field lines is important because the magnetic field produces emission that contributes to infrared variability usually connected to atmospheric clouds. With these detections, they were able to show that the strong

magnetic fields of their subjects could not be accounted for by the age, mass, and temperature of those objects, making the rotational effects on magnetism more prominent. This group found the same mass and period for SIMPJ0136, making it the "first planetary-mass object detected in the radio", and indicated the possibility of SIMPJ0136 being a rogue exoplanet.

Using the observations of past research of SIMPJ0136, we will determine how its atmosphere changed over the course of 3 epochs, starting in 2013. We will analyze its light curves and spectra over these three different time periods and determine the most likely scenario of atmospheric composition.

2 Analysis of Observational Data

2.1 Observational Data

The first part of our exploration will be to recreate the research done by the team led by Apai in 2013, as well as to perform the same spectral and light curve visualizations on more recent data taken of the brown dwarf. The three sets of data were taken with the Hubble Space Telescope's Wide Field Camera 3 Instrument. The first set consists of 495 spectra from over the course of 8 hours, where each spectrum was integrated over 22.34 seconds. The second epoch of data was taken in September of 2013, and the third in October of 2013. These sets of data consist of spectra from over the course of 4 hours each and the spectra were integrated over 22.34 seconds. Because the target is a relatively bright 13.5-magnitude light source, a high signal-to-noise ratio was able to be captured in all three epochs. These time-series spectroscopic data will help us analyze the long-term weather evolution of SIMPJ0136.

2.2 Time-Series Spectra and Light Curves

Using the same Hubble Space Telescope data that were used to visualize periods of SIMPJ0136 in the work of Apai et al., we reproduce their data analyses, creating light curves and analyzing spectral differences over approximately 3 periods of rotations from SIMPJ0136.

To obtain light curves from the time series spectra recorded of the brown dwarf, we develop

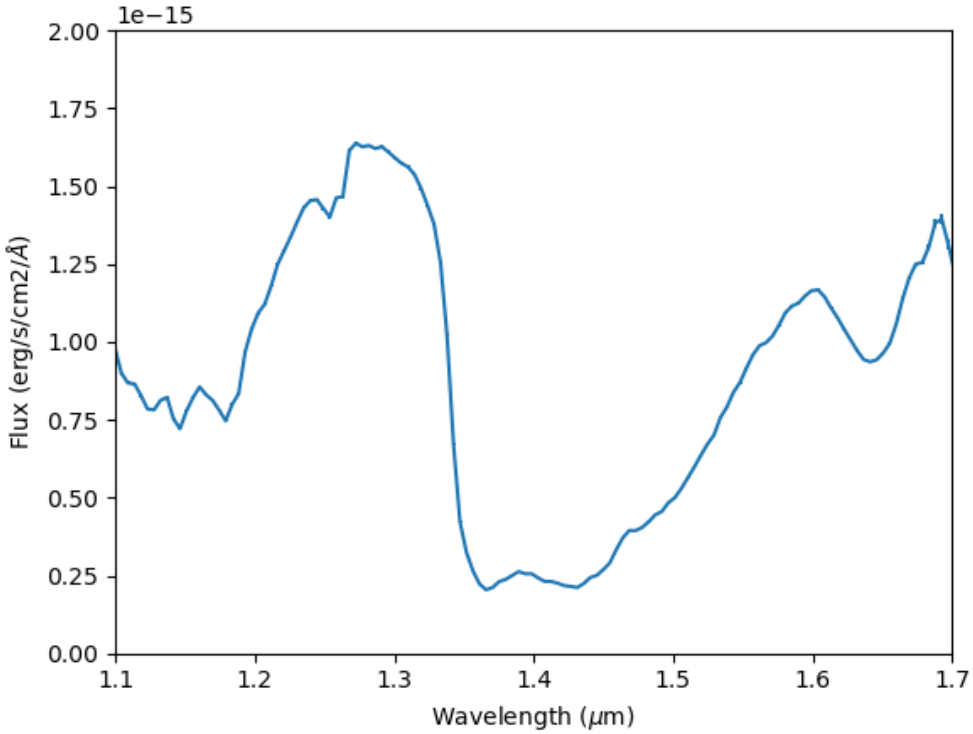

Figure 4: The first spectrum taken of the brown dwarf in Epoch 1. The spectrum shows a maximum between 1.27 and 1.31 micrometers, and a minimum between 1.37 and 1.43 micrometers. There are also double sodium absorption lines present at approximately 1.26 micrometers.

code employing NumPy and SciPy libraries to import, read, and visualize the spectral datacubes [11][12]. This data contains four parameters: the Julien Date of observation, the wavelength of light recorded, a 2D array of spectra that stores time and wavelength, and the errors for this array. Plotting spectra, then, can be done by choosing one of the spectra taken from the array. Light curves can be plotted by integrating the flux found over a specific range of wavelengths.

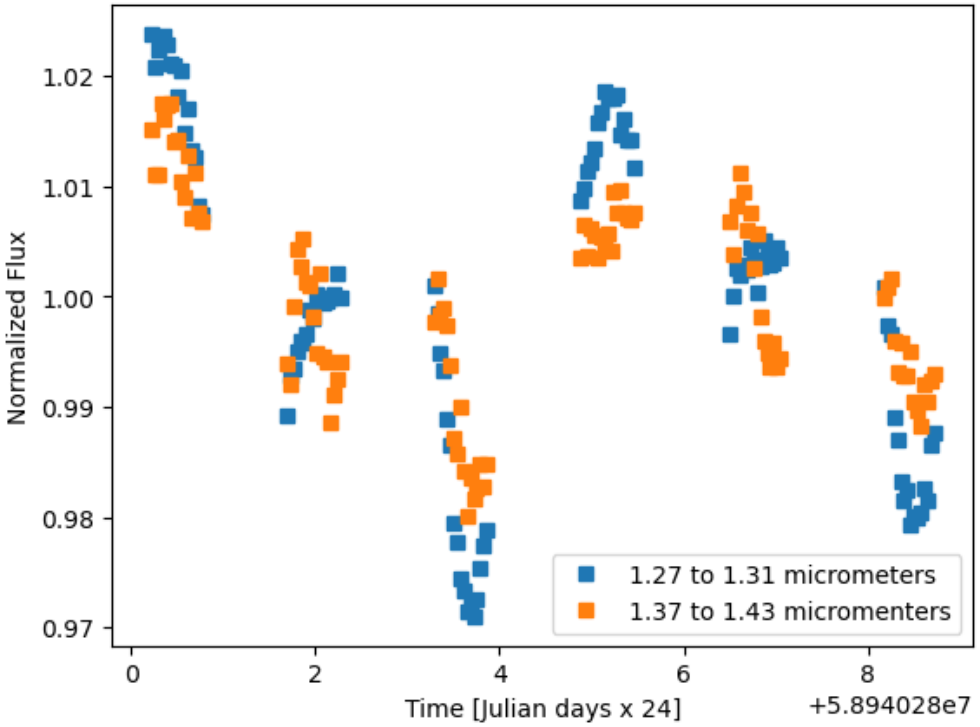

Figure 5: Normalized light curves from Epoch 1 integrated over different wavelength bands. The blue data is from light integrated over the range of wavelengths associated with the maximum in the spectrum, and the orange data is from light integrated over the minimum, whose range of wavelengths is associated with water absorption. The blue light curve has a relatively higher variance than the orange light curve for most of its peaks and troughs.

In Figure 4, the maximum flux occurs between 1.27 and 1.31 micrometers, while the minimum flux occurs between 1.37 and 1.43 micrometers. Sodium absorption lines can be seen near the maximum, and the minimum points to water absorption. We plot light curves integrated over the bounds related to these extrema to visualize the observed changes in flux from the brown dwarf bound within these wavelengths of light. This can be seen in Figure 5, where the changes in wavelength band integration affect the overall variations in the maxima and minima of the light curves, but do not affect the general shape or frequency of extrema. Since the flux difference is so high between these wavelength bands, the fluxes can instead be normalized with their averages to emphasize the relative differences between each band instead of the exact. The observed differences may point to cloud presence in the atmosphere, where the blue plotted line is flux that comes from deeper within the atmosphere, and the orange line is from bands of wavelengths that penetrate the atmosphere less than those in blue. However, these differences in cloud opacities are not constant; one orange maximum exceeds the blue maximum and one is relatively equal. This imperfect peri-

odicity might be attributed to changing weather patterns between rotations of the brown dwarf, a storm, or possibly even magnetic fields and auroras, as explained by Kao et al. in 2018 [10].

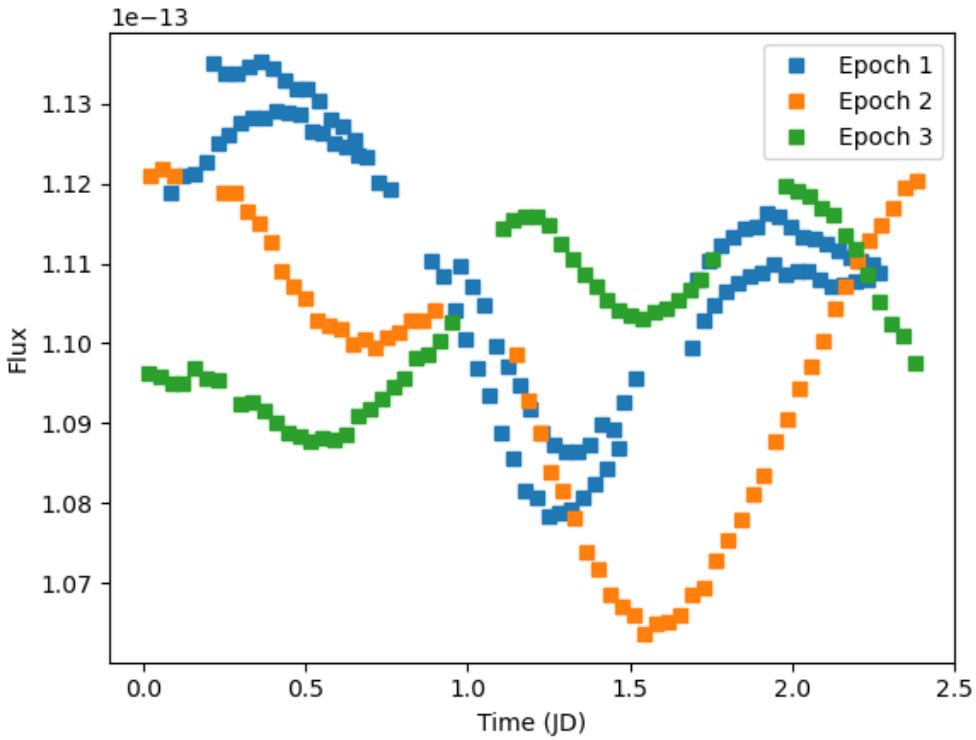

Figure 6: Folded light curves from the three epochs. Epoch 1 is plotted in blue, Epoch 2 in orange, and Epoch 3 in green. Epoch 1 and 2 show similar variance, while Epoch 3's data show a smaller range of flux values. These light curves indicate the possibility that in Epoch 1, one thick patch of clouds is present in the atmosphere, while in Epoch 2 and 3 two thick patches are present. The difference in thickness of the clouds in Epoch 3 may be smaller than the difference in thickness of the clouds in Epochs 1 and 2.

Similar non-periodicity is found in the other two epochs. The phase folded light curves of each epoch, shown in Figure 6, are constructed over 1.1 to 1.7 micrometer wavelengths of light. The folded light curves are constructed assuming a 2.4 hour period of rotation, consistent with previously stated periods of rotation from scientific papers studying SIMPJ0136. Qualitatively, Epoch 1 and 2 experience similar flux variations, while Epoch 3's extrema are closer to the median flux. This indicates that the thickness of clouds across its surface is not as highly variant as those of Epochs 1 and 2. Meanwhile, the variations in the number of extrema between the epochs point to variations in the number of "patches" of thicker or thinner clouds in the atmosphere. Epoch 1, for example, has one minima compared to Epoch 2 which has 2 minima. It can be deduced then, that Epoch 1 may have at least one patch of thicker clouds on its surface while Epoch 2 has two or more patches. Epoch 3's cloud thickness is more evenly distributed but also has two thicker areas of clouds. The minima are associated with thicker clouds because they lessen the light coming from the brown dwarf.

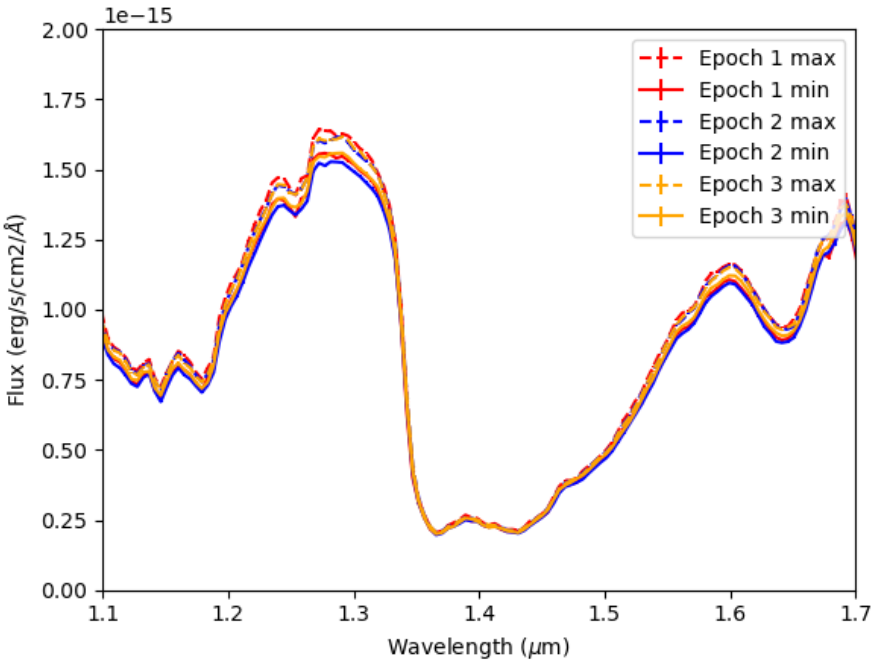

Figure 7: The maximum and minimum spectrum from each Epoch. Epoch 1 data is plotted in red, Epoch 2 in blue, and Epoch 3 in yellow. Maximums are plotted as dotted lines while minimums are solid. The greatest variations occur in the maxima of the spectra both between and in each epoch. Variations are notably greater within the same epochs than between different epochs.

Using the NumPy library, we create code to parse through each spectrum in Epochs 1, 2, and 3. Our code creates an array containing the maximum flux values measured at each wavelength, labeled as our "maximum spectrum". We repeat this process for our "minimum spectrum" [11]. The resultant maximum and minimum spectra from each epoch are shown in Figure 7.

Figure 7 shows that while the key elements of the maximum and minimum spectra are unchanging, there are still some flux variations present. The flux varies mainly between 1.25 and 1.3 micrometers, or the maximum, while the flux collected between wavelengths 1.37 and 1.43, or the minimum, is consistent both between each of the epochs and between the maximums and minimums of each epoch. Spectral variations within each epoch point to differences in cloud thickness in the epochs. To compare these differences, a ratio between the maximum and minimum spectra is plotted for each epoch. These graphs are made to identify the relative changes in spectral flux when comparing the maximum and minimum spectra of each epoch. Figure 8 presents the ratios of the mean of the 5 brightest spectra from each epoch over the mean of the 5 faintest spectra.

The spectral ratios from Epochs 1 and 2 are nearly identical, which points to a lack of changes in the variations of thickness among the clouds between these two epochs. Epoch 3, on the other hand, shows a much smaller variation between its maximum and minimum ratios. The dip in the ratio indicates a change in the cloud altitudes. The similarity between Epochs 1 and 2 is notable because these observations were taken nearly 2 Earth years apart, equivalent to around 7,000 rotations of the brown dwarf.

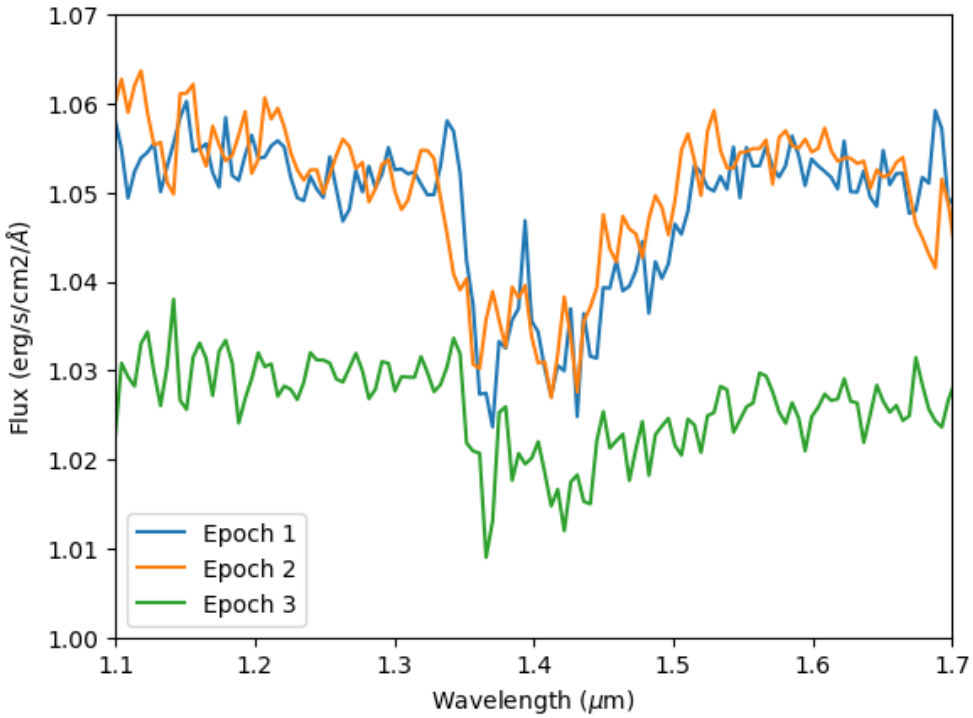

Figure 8: Ratios of mean of 5 brightest spectra over mean of 5 faintest spectra from each epoch. Epoch 1 is plotted in blue, Epoch 2 in orange, and Epoch 3 in green. Epochs 1 and 2 are notably similar, pointing to a similarity of variations in cloud thicknesses between the epochs. Epoch 3 has a lower ratio, which indicates a change in cloud altitudes. The general shape of the plots are similar between the three epochs, with a dip in the water band between 1.37 and 1.43 micrometers.

3 Atmospheric Models

In this section, we compare observational data to atmospheric models to explore the possible origins of the observed variability. We determine how clouds and temperature may affect light curve fluctuations, and then utilize chi-square best-fit modeling to determine a probable atmosphere of the brown dwarf.

3.1 Clouds, Flux, and Temperature

To start to explain the spectral and light curve variability, we can construct a simple model to understand the effect of temperature variances on a blackbody. Specifically, we want to visualize how observed flux may change with the presence of a cold spot in the atmosphere. By creating a model that visualizes the changes in flux that can occur from the presence of a spot in an atmosphere with differing temperatures and coverage areas, we can identify what inputs are required to recreate the changes in flux observed in Epochs 1, 2, and 3.

Our model begins with Hemisphere 1 of a blackbody, which is covered in a temperature $T0$. Hemisphere 1 produces a higher flux than Hemisphere 2, which is mostly covered with a temperature $T0$ except for a circular patch which is covered in temperature $T1$. By assuming these hemispheres operate as blackbodies, the Stefan Boltzmann law can be used to calculate the flux variance (Δflux) between the two hemispheres:

$$\Delta\text{flux} = \frac{2\alpha(T_0^4 - T_1^4)}{(2-\alpha)T_0^4 + \alpha T_0^4}, \tag{1}$$

where α is the percentage of Hemisphere 2 at $T1$, $T0$ is the temperature covering most of the blackbody, and $T1$ is the temperature of the cold spot.

With this equation and data from each epoch, we can graph a 2D plot whose parameters include the temperature of the cold spot in the atmosphere and the percentage of the planet that this spot covers. The output graphed in Figure 9 is the change in flux that may be observed as the planet rotates. Data from Epochs 1, 2, and 3 are plotted on top of this plot, showing the general predicted cloud coverage percentage for a set of three possible assumed temperatures. $T0$ was assumed to be 1000K to reproduce the differences in peaks and troughs of light curve analyses over the epochs. It is important to note that this graph is a very simplified model only used to explain how these chosen parameters may cause observed variability changes. A blackbody function cannot accurately represent the real spectrum of a brown dwarf because it does not account for factors like clouds, atmospheric compositions, or any other factors that affect spectra.

Figure 9 shows that a higher temperature contrast between the spot and the rest of the atmosphere causes a higher change in flux, as does a higher surface area of the cold spot, or "cloud coverage". Since this model is based on a blackbody, it can only reproduce observed flux changes in light curves, not in spectra. We must build a realistic model of the atmosphere to determine real predictions for cloud coverage percentages, which will be done using chi-square statistics and model data.

3.2 Model Fitting

Using model data parameterized by cloud thickness and temperature, we find atmospheric qualities that present spectra most similar to our observations. The derived models are created using the

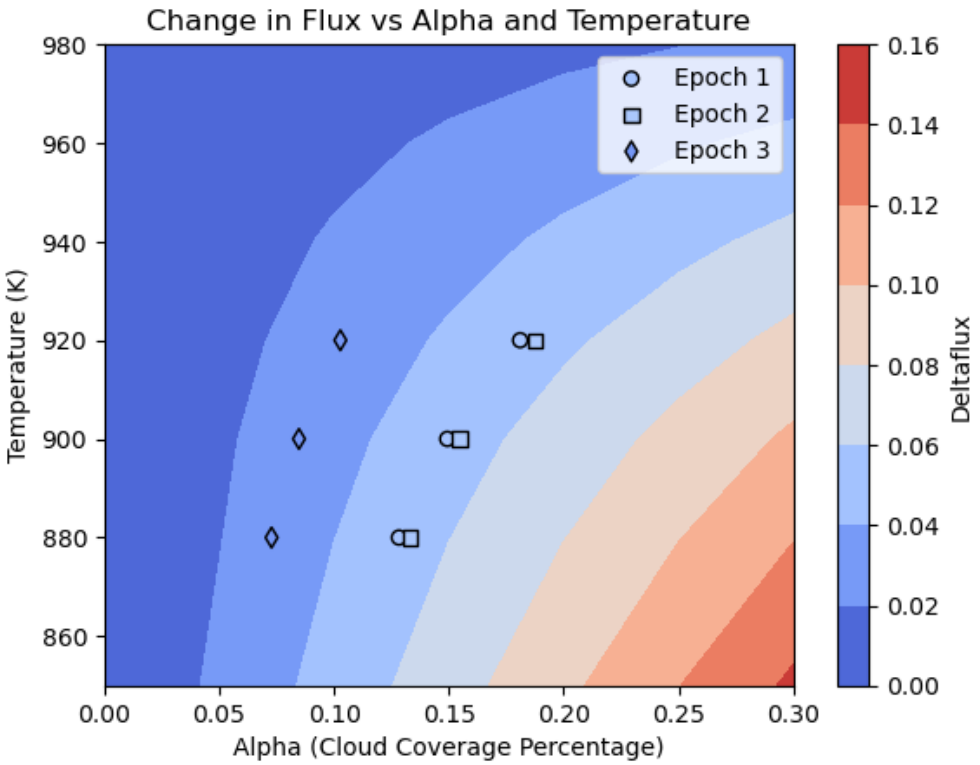

Figure 9: 2D Plot of flux change as a function of a cold spot's temperature and coverage percentage on a blackbody of 1000K. This graph shows possible variations between temperature and cloud coverage to produce fluctuations in observed light flux. Change in flux derived from actual observations along with three assumed temperatures are used to determine the required spot coverage percentage of colder "clouds" in the atmosphere. Change in flux is graphed as background color, where bluer shades are low flux and redder shades are higher. The assumed temperature of the overall blackbody is 1000K, and the Y axis presents temperatures of the spot of colder atmosphere on the blackbody. The X axis is the percentage of one hemisphere that the spot covers. Epoch 1 data is represented with circles, Epoch 2 with squares, and Epoch 3 with diamonds. These shapes are colored to indicate the change in flux that they experience. To reproduce the observed changes in flux from the epochs, and assuming some key temperatures, Epochs 1 and 2 would need greater cloud coverage than Epoch 1, by around 5 percent.

Picaso code [13]. Figures 10 and 11 present model data that vary by cloud thickness and temperature, respectively. We use these models to better understand the behaviors of this brown dwarf model regarding the relation of temperature and cloud thickness on spectral shape. To find the parameters that lead to a model of best fit to our observations, we can use chi-square statistics.

The chi-square formula, as seen in equation 2 is used in statistics to quantify the difference between observational data and model predictions. The chi-square statistic, which will determine the best-fitting model for our data, can be calculated using this formula:

$$\chi^2 = \sum_i \frac{(O_i - M_i)^2}{E_i^2}, \tag{2}$$

where O represents observational data points, M represents theoretical model points, and E is estimated error. A smaller chi-square statistic indicates a better fit to the observational data.
In Figure 10, the atmosphere is set to 1200K while the cloud type changes. With clear clouds, there are obvious sodium absorption lines at around 1.24 microns. Along with the disappearance of the sodium lines, models with thicker clouds show a relatively higher flux at longer wavelengths. This is because longer wavelengths are able to penetrate layers of dust better than shorter wavelengths. Due to this property of light, the spectra with thicker cloud layers demonstrate a much higher relative flux in the longer wavelengths and a decrease in relative flux in the shorter wavelengths.

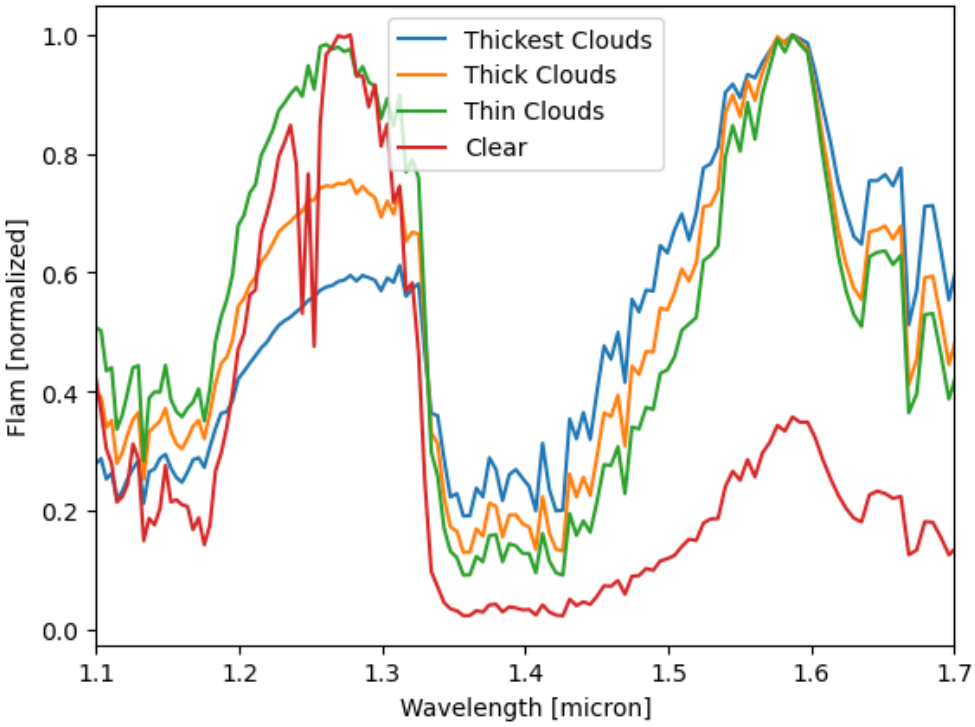

Figure 10: Normalized model spectra of an atmosphere of 1200K with varying cloud conditions. The model with the thickest clouds is plotted in blue, thick clouds in orange, thin clouds in green, and no clouds in red. The atmosphere with no clouds shows prominent sodium absorption lines, and has a significantly lower secondary peak. As the clouds thicken, the fluxes produced from lower wavelengths lessen relative to the higher wavelengths.

In Figure 11, an atmosphere is covered by thin clouds while the temperature changes. Although the first peak of the spectra found at the shorter wavelengths is noticeably similar among the atmospheres with different temperatures, the second maximum and the minima differ significantly. Specifically, as the temperature gets higher, the minima increase, indicating weaker water absorption bands. As for the maxima, the unchanging peak of the blackbody is surprising. Intuitively, as the temperature of the brown dwarf increases, the flux of both maxima should increase in the spectrum. However, this does not occur; only the second peak increases with temperature. This is because of the opacity of clouds and water, which change in the infrared and the visible spectrum of light.

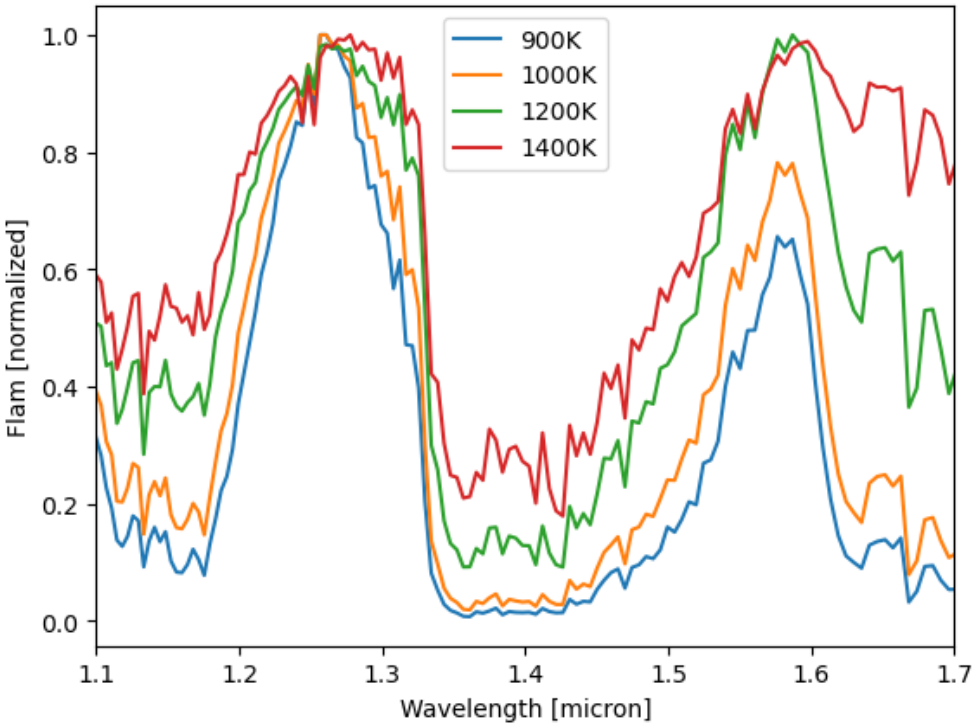

Figure 11: Normalized model spectra of an atmosphere composed of thin clouds with varying temperatures. The model with an atmosphere of 900K is plotted in blue, 1000K in orange, 1200K in green, and 1400K in red. The plot shows a widening first peak as the temperature rises, and a directly proportional relationship between the second peak of flux and temperature.

Plotting our observational data, we create code to run chi-square statistics on possible models and choose the best combined parameters to describe our observational data. The best-fit model for all three epochs are thin clouds at 1200K. The fitted model for Epoch 1 is shown in Figure 12, and is very similar to the fits for Epochs 2 and 3.

It is clear that even the best-fitting model, Figure 12, is not a perfect fit for our observational data. The second maximum seen in the observational data peaks much lower than that of the model. This indicates the potential presence of a patch of thicker clouds somewhere in the atmosphere, as thicker clouds increase the relative flux of the second maximum to the first, as shown by Figure 10.

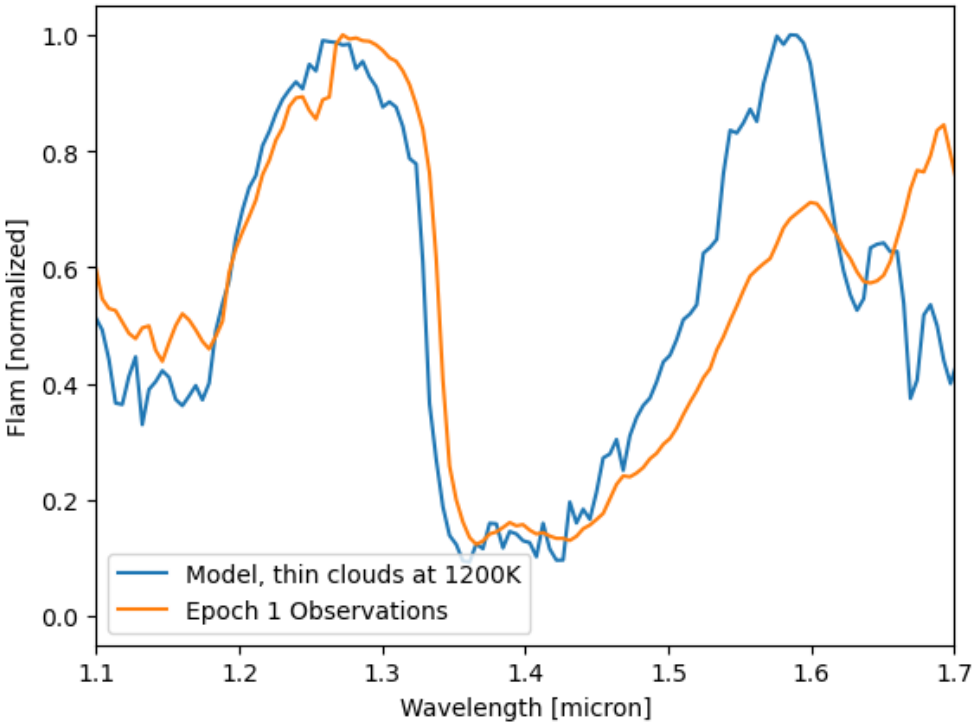

Figure 12: Model spectrum that best fits our Epoch 1 observational spectra. The model spectrum is plotted in blue, and the observational spectrum is plotted in orange. The shorter wavelengths present a decent fit to the observational data, but for the longer wavelengths the model data is notably lower. To provide a more accurate fit, we must produce a model that accounts for some deviation in the atmosphere, whether in cloud thickness or in temperature.

3.3 Deviation Model Fitting

Because of the heightened deviation from the model plot in Figure 12, we can determine that there must be some deviation from an atmosphere of thin, 1200K clouds. To determine how or whether this patch of atmosphere differs in temperature and/or cloud thickness, we can compare the shapes of varying ratio plots to Figure 13, which presents the ratios of the mean of the 5 brightest spectra from each epoch over the mean of the 5 faintest spectra. Figure 13 is characterized by a general shape in which the ratio is relatively stable except for a dip in the water band from 1.37 to 1.43 micrometers. To find the best characteristics of our varied spot in the atmosphere, we can create ratio plots of potential candidates with model data to find a shape most similar to that in Figure 13.

In analyzing the general shapes of the produced ratio plots in Figure 14, it can be seen that the orange and blue lines, where the temperature was changed, create minima where Figure 13 shows maxima, and create maxima where Figure 13 show minima. Thus, we conclude that the divergent spot should not differ in temperature from the rest of the atmosphere. The red line, which shows the effect of a clear patch of atmosphere on the brown dwarf, follows the general directions of Figure 13. However, the 1.2 to 1.3 micron wavelength range shows a much greater maximum than the maximum in 1.5 to 1.7 microns, which should be approximately equal to its shorter wavelength counterpart. Also, double sodium lines are prominent and extremely pronounced in the red ratio line, that of which are not present in the observed spectra ratio. Thus, there should be no cloudless spots in the atmosphere on the brown dwarf. Through the process of elimination, we can deduce that the noted abnormalities in our model spectra may be due to a patch of thicker clouds in the atmosphere otherwise covered in thin, 1200K clouds.

To find the percentage of the atmosphere covered in thick clouds, we can again use the chi-square formula seen in equation 2. Assuming that SIMPJ0136 radiates as a blackbody, we can develop equation 3,

$$H2 = \alpha \times \text{model flux} + \alpha \times H1 \tag{3}$$

where $H1$ is the flux that radiates from the hemisphere covered only in thin clouds and $H2$ is the flux that radiates from the other hemisphere, which contains a thicker cloud of patches that covers an α percentage of the surface area of $H2$.

By creating a code that runs through each possible alpha and generates a corresponding chi value, we can plot the least-chi alpha and determine the best-fitting atmospheric model. The ratio plots of observed data from Epochs 1, 2, and 3 are plotted against their respective best-fit models in figures 15, 16, and 17.

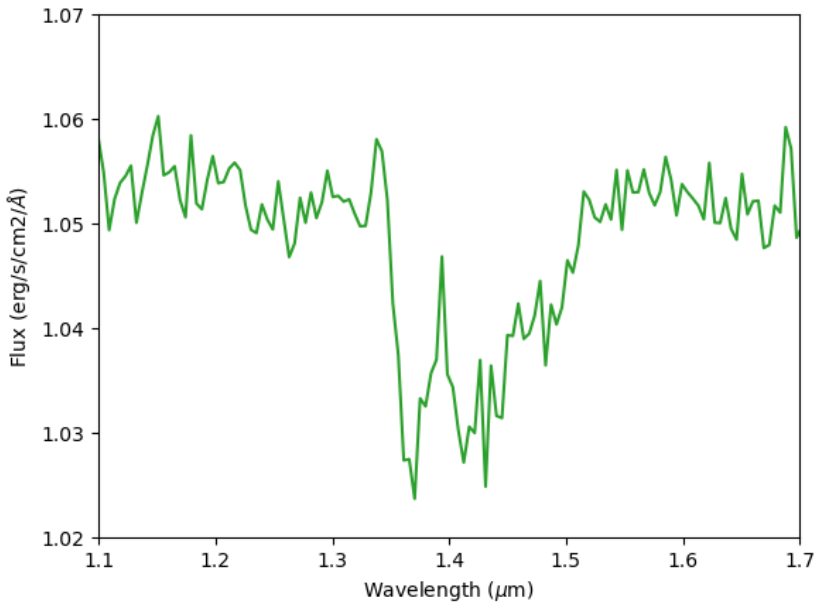

Figure 13: Ratio plot of the mean of the 5 brightest spectra over the mean of the 5 faintest spectra in Epoch 1. This is the same plot from Figure 8, but enlarged to emphasize the desired shape from potential ratio plots created in Figure 14.

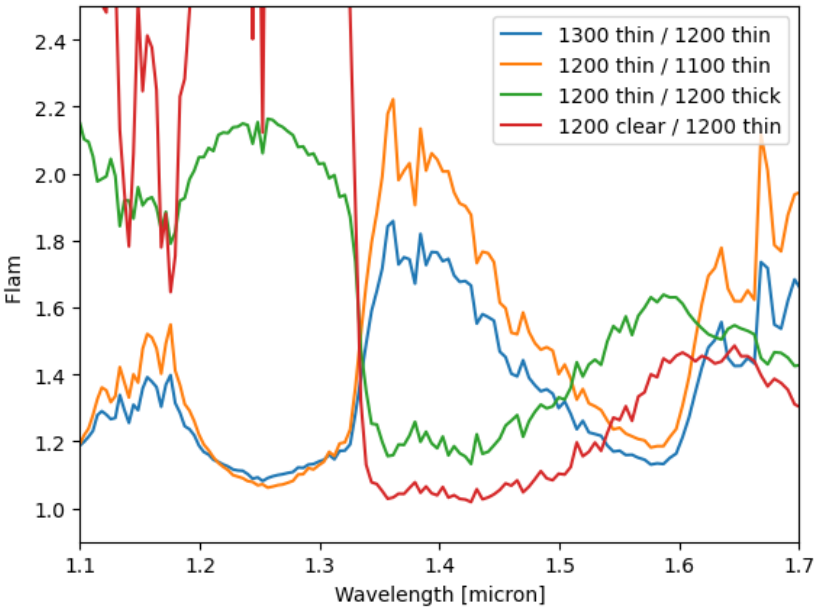

Figure 14: Ratio plots of model spectra with varied temperatures and cloud thicknesses. The ratio of a 1300K atmosphere with thin clouds over a 1200K atmosphere with thin clouds is plotted in blue. The ratio of a 1200K atmosphere with thin clouds over a 1100K atmosphere with thin clouds is plotted in orange. The ratio of a 1200K atmosphere with thin clouds over a 1200K atmosphere with thick clouds is plotted in green. The ratio of a 1200K atmosphere with no clouds over a 1200K atmosphere with thin clouds is plotted in red. Only ratios that could produce a positive output are plotted, as Figure 13 is positive. The green line is of most similar shape to the plot in figure 13, and thus is the candidate for the distinct spot in our atmosphere.

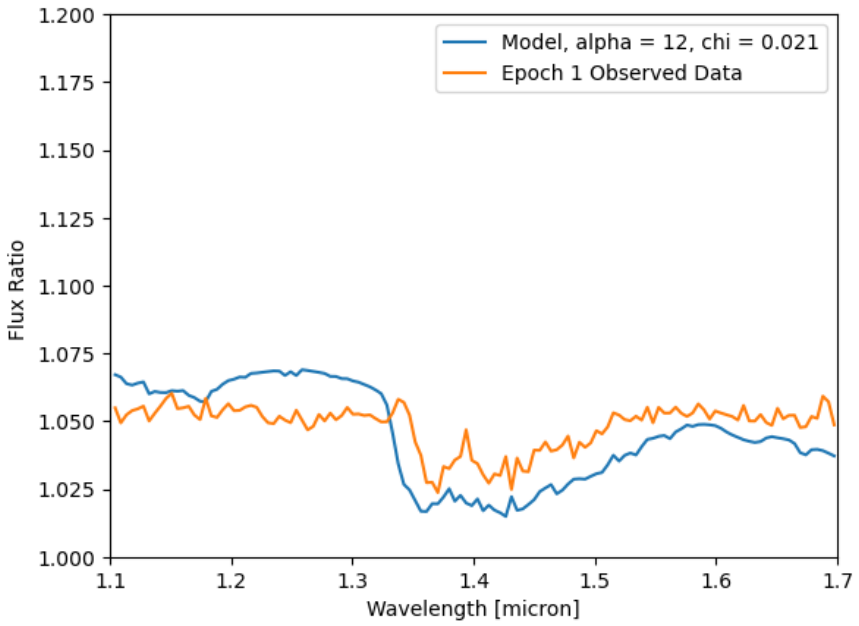

Figure 15: Epoch 1 model of best fit. The model is plotted in blue, and the observed data is plotted in orange. The observed data is the ratio between the mean of the 5 brightest spectra over the mean of the 5 faintest spectra. The model of best fit is a ratio model based on equation 3 in which 12 percent of one hemisphere is covered in thick, 1200K clouds in an atmosphere that it otherwise covered in thin, 1200K clouds.

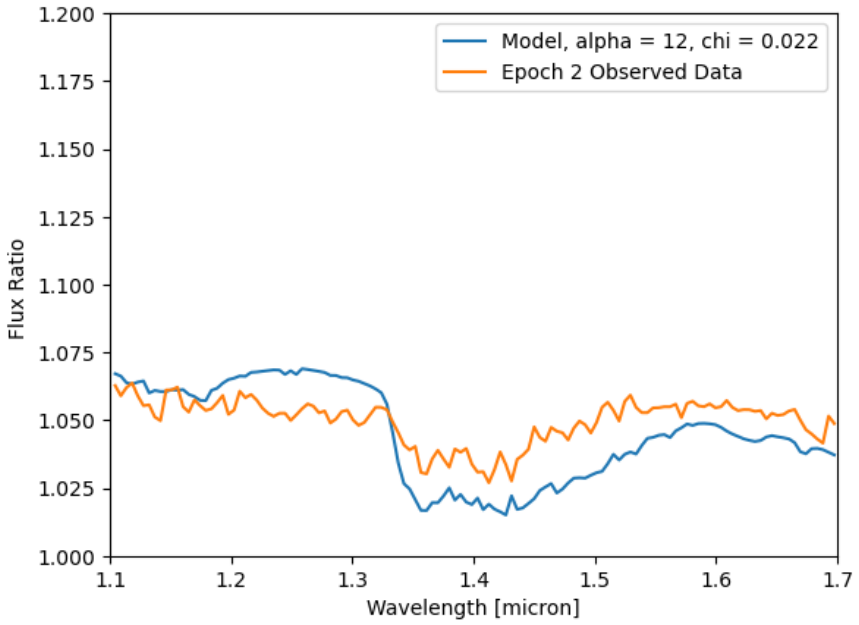

Figure 16: Epoch 2 model of best fit. The model is plotted in blue, and the observed data is plotted in orange. The observed data is the ratio between the mean of the 5 brightest spectra over the mean of the 5 faintest spectra. The model of best fit is a ratio model based on equation 3 in which 12 percent of one hemisphere is covered in thick, 1200K clouds in an atmosphere that it otherwise covered in thin, 1200K clouds.

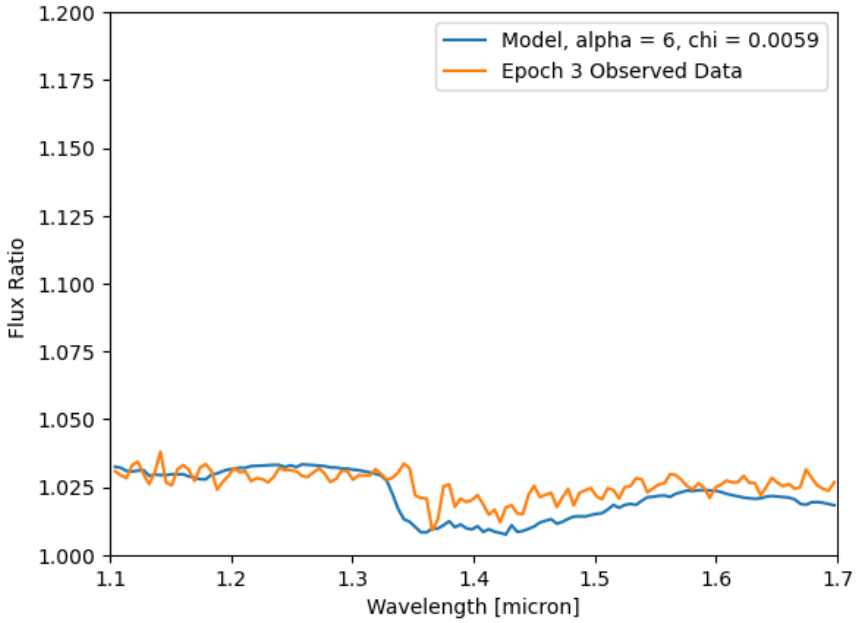

Figure 17: Epoch 3 model of best fit. The model is plotted in blue, and the observed data is plotted in orange. The observed data is the ratio between the mean of the 5 brightest spectra over the mean of the 5 faintest spectra. The model of best fit is a ratio model based on equation 3 in which 6 percent of one hemisphere is covered in thick, 1200K clouds in an atmosphere that it otherwise covered in thin, 1200K clouds. Compared with the first two epochs, this model fit is most accurate among the three.

4 Results and Conclusion

Our results not only reinforce and align with past findings from the group of researchers in 2013, but expand on this data into two more eras of weather pattern roughly 7000 rotations apart from the first studied epoch. In all of the epochs, the brown dwarf was found to have an atmosphere completely covered in thin, 1200K clouds with some surface area covered by thicker clouds as well. The exact percentage of thicker clouds was found using ratio plots, which provided better fits to the observational than regular spectral models, as the ratio models explain variations rather than absolute flux. This thicker patch of clouds was found to make up 12 percent of one hemisphere in both Epochs 1 and 2, and 6 percent in Epoch 3. Epoch 3 overall was found to have less variance among its spectra, as shown by its spectral ratio plot. Epoch 3 also had the least chi-square value, meaning the model was the most accurate out of the three epochs.

These results, along with past data collected from SIMPJ0136, allow us to present a timeline of weather and climate structure in the atmosphere of the brown dwarf. Light curve analysis agreed with past observations of a 2.4 hour period. Over the three epochs, this period is consistent. The shape of the curves, however, is not. The first two epochs show greater variation in their ranges of flux, while Epoch 3 has more peaks and thus indicates a more complex weather pattern. Although the light curve structures vary heavily between the three epochs, the shape of the spectra ratio plots are extremely similar. All three epochs show a dip in the water band, indicating that the components of the clouds do not differ between epochs. Spectral analysis also indicates a great difference between the first two epochs and the third. When comparing maximum over minimum spectra ratios from each epoch, it can be seen that, although the pattern is similar between all three epochs, the variations are much more subtle in the last epoch.

Based on this data, it is clear that over the past decade, the climate of SIMPJ0136 has remained relatively stable. The atmosphere is covered in thin, 1200K clouds with some thicker clouds interspersed, covering only 12 percent of a hemisphere in the first two epochs and 6 percent of a hemisphere in the third epoch. Our findings agree with the findings from the 2013 research study, whose conclusions included that the brown dwarf is covered in a layer of thin clouds with a patch of thicker clouds as well.

Our findings can be summarized below:

- The light curves are consistent with a previously observed period of rotation of 2.4 hours.
- Light curve patterns indicate patchy atmospheres in all three epochs. Epoch 3 shows the most complex patterns, indicating a more complex cloud structure. It also shows less variability in flux, indicating less variation in cloud thicknesses.
- The observed variability in flux from Epochs 1, 2, and 3 are wavelength dependent.
- Between data taken between two Earth years, or approximately 7000 rotations of the brown dwarf, the average flux change is less than those observed within a single rotation.
- Observed spectra are consistent with an atmosphere covered in thin, 1200K clouds with a patch of thicker clouds in each epoch. There should be no clear patches, uncovered by clouds, in the atmosphere of any of the epochs.
- In Epochs 1 and 2, the percentage of one hemisphere of the brown dwarf covered by thicker clouds is 12 percent, and in Epoch 3, the percentage of one hemisphere covered by thicker

clouds is 6 percent. Epochs 1 and 2 have consistent cloud coverage and Epoch 3 has a lower cloud coverage.

- We find that the average spectral appearance of this brown dwarf is consistent across 3 epochs, but also find strong evidence of the cloud coverage fraction changing. The cloud type did not change across the 3 epochs, but the patterns and coverage did.

5 Acknowledgements

The author of this senior thesis would like to thank Dr. Yifan Zhou for being an amazing research supervisor. His kindness, flexibility, and ability to explain hard concepts helped this semester of research go by smoothly. She would also like to thank the Department of Astronomy, all of the professors that she has had the privilege to take classes from, and Gabby Fuller. Finally, she would like to thank her family, her roommates, and her cat, Mikan.

References

[1] Michael Perryman. "The Exoplanet Handbook". In: (2018), pp. 1–16.

[2] Jacqueline K. Faherty et al. "POPULATION PROPERTIES OF BROWN DWARF ANALOGS TO EXOPLANETS*". In: *The Astrophysical Journal Supplement Series* 225.1 (July 2016), p. 10. DOI: 10.3847/0067-0049/225/1/10. URL: https://dx.doi.org/10.3847/0067-0049/225/1/10.

[3] Brendan P. Bowler. "Imaging Extrasolar Giant Planets". In: *Publications of the Astronomical Society of the Pacific* 128.968 (Aug. 2016), p. 102001. ISSN: 1538-3873. DOI: 10.1088/1538-3873/128/968/102001. URL: http://dx.doi.org/10.1088/1538-3873/128/968/102001.

[4] Jacqueline K. Faherty et al. "2MASS J035523.37+113343.7: A YOUNG, DUSTY, NEARBY, ISOLATED BROWN DWARF RESEMBLING A GIANT EXOPLANET". In: *The Astronomical Journal* 145.1 (Nov. 2012), p. 2. DOI: 10.1088/0004-6256/145/1/2. URL: https://dx.doi.org/10.1088/0004-6256/145/1/2.

[5] Jonathan Gagne et al. "SIMP J013656.5+093347 Is Likely a Planetary-mass Object in the Carina-Near Moving Group". In: *The Astrophysical Journal Letters* 841.1 (May 2017), p. L1. DOI: 10.3847/2041-8213/aa70e2. URL: https://dx.doi.org/10.3847/2041-8213/aa70e2.

[6] Nikku Madhusudhan. "Exoplanetary Atmospheres: Key Insights, Challenges, and Prospects". In: *Annual Review of Astronomy and Astrophysics* 57.Volume 57, 2019 (2019), pp. 617–663. ISSN: 1545-4282. DOI: https://doi.org/10.1146/annurev-astro-081817-051846. URL: https://www.annualreviews.org/content/journals/10.1146/annurev-astro-081817-051846.

[7] M. S. Marley et al. "Clouds and hazes in exoplanet atmospheres". In: *Comparative Climatology of Terrestrial Planets*. Ed. by S. J. Mackwell et al. Space Science Series. Phoenix: University of Arizona Press, 2013, pp. 367–391. DOI: 10.2458/azu_uapress_9780816530595-ch015.

[8] Étienne Artigau et al. "PHOTOMETRIC VARIABILITY OF THE T2.5 BROWN DWARF SIMP J013656.5+093347: EVIDENCE FOR EVOLVING WEATHER PATTERNS". In: *The Astrophysical Journal* 701.2 (Aug. 2009), p. 1534. DOI: 10.1088/0004-637X/701/2/1534. URL: https://dx.doi.org/10.1088/0004-637X/701/2/1534.

[9] Dániel Apai et al. "HST SPECTRAL MAPPING OF L/T TRANSITION BROWN DWARFS REVEALS CLOUD THICKNESS VARIATIONS". In: *The Astrophysical Journal* 768.2 (Apr. 2013), p. 121. DOI: 10.1088/0004-637X/768/2/121. URL: https://dx.doi.org/10.1088/0004-637X/768/2/121.

[10] Melodie M. Kao et al. "The Strongest Magnetic Fields on the Coolest Brown Dwarfs". In: *The Astrophysical Journal Supplement Series* 237.2 (July 2018), p. 25. DOI: 10.3847/1538-4365/aac2d5. URL: https://dx.doi.org/10.3847/1538-4365/aac2d5.

[11] Charles R. Harris et al. "Array programming with NumPy". In: *Nature* 585.7825 (Sept. 2020), pp. 357–362. DOI: 10.1038/s41586-020-2649-2. URL: https://doi.org/10.1038/s41586-020-2649-2.

[12] Pauli Virtanen et al. "SciPy 1.0: Fundamental Algorithms for Scientific Computing in Python". In: *Nature Methods* 17 (2020), pp. 261–272. DOI: 10.1038/s41592-019-0686-2.

[13] Sagnick Mukherjee et al. "PICASO 3.0: A One-dimensional Climate Model for Giant Planets and Brown Dwarfs". In: *The Astrophysical Journal* 942.2 (Jan. 2023), p. 71. DOI: 10.3847/1538-4357/ac9f48. URL: https://dx.doi.org/10.3847/1538-4357/ac9f48.